Magnetron sputter deposition of silver onto castor oil: the effect of plasma parameters on nanoparticle properties

Anastasiya P. Sergievskaya [1], Amy O'Reilly [1], Adrien Chauvin [2], Jozef Veselý [3], Adriano Panepinto [1], Julien De Winter [4], David Cornil [5], Jérôme Cornil [5], Stéphanos Konstantinidis [1*]*

[1] Chemistry of Plasma-Surface Interactions (ChIPS), CIRMAP, Research Institute for Materials Science and Engineering, University of Mons, 23 Place du Parc, B-7000 Mons, Belgium

[2] Department of Condensed Matter Physics, Faculty of Mathematics and Physics, Charles University, Ke Karlovu 5, 121 16 Praha 2, Czech Republic

[3] Department of Physics of Materials, Faculty of Mathematics and Physics, Charles University, Ke Karlovu 5, 121 16 Praha 2, Czech Republic

[4] Organic Synthesis and Mass Spectrometry Laboratory (S²MOs), University of Mons, 23 Place du Parc, B-7000 Mons, Belgium

[5] Laboratory for Chemistry of Novel Materials (CMN), University of Mons, Place du Parc 23, Mons 7000, Belgium

* corresponding authors

ORCID / e-mails:

A. Sergievskaya https://orcid.org/0000-0001-9589-9546 / anastasiya.sergievskaya@umons.ac.be
A. O'Reilly oreila20@tcd.ie
A. Chauvin https://orcid.org/0000-0003-1896-8776 / andrien.chauvin@karlov.mff.cuni.cz
J. Veselý https://orcid.org/0000-0002-7395-0301 / vesely@gjh.sk
A. Panepinto https://orcid.org/0000-0002-5133-5834 / adriano.panepinto@umons.ac.be
J. De Winter https://orcid.org/0000-0003-3429-5911 / julien.dewinter@umons.ac.be
D. Cornil https://orcid.org/0000-0002-9553-1626 / david.cornil@umons.ac.be
J. Cornil https://orcid.org/0000-0002-5479-4227 / jerome.cornil@umons.ac.be
S. Konstantinidis https://orcid.org/0000-0002-1672-309X / stephanos.konstantinidis@umons.be

KEYWORDS: silver nanoparticles, castor oil, magnetron sputtering onto liquids.

ABSTRACT Magnetron sputter deposition of metals onto low vapor pressure liquids is a clean and simple method of nanoparticle (NP) production. Herein, we discuss the production of silver nanoparticles (Ag NPs) via direct current magnetron sputtering (DC-MS) and high-power impulse magnetron sputtering (HiPIMS) of a silver target onto biocompatible and highly available liquid, castor oil. Effect of sputtering parameters such a sputter time, applied power, working gas pressure and type of sputtering plasma onto NP properties has been studied by UV-vis spectroscopy and transmission electron microscopy (TEM). The scenario of Ag NPs formation is drawn from these analyses, supported by mass-spectrometry and quantum-chemistry based calculations. Initial Ag NPs formed in castor oil have diameter from 0.8 nm to 4 nm and tend to form aggregates.

INTRODUCTION

Synthesis of metal nanoparticles (NPs) stays a topic of intense research due to their unique properties making them highly promising for potential applications in electronics, catalysis, molecular sensing and biomedicine [1]. Even though thousands of different synthetic procedures were designed in the last 30 years, most of the recipes has never been adapted for large scale

production because of the high sensitivity of the process to minor changes in the experimental conditions. Reproducibility still is one of the most important problems in nanomaterial production and often scaling up the desired synthetic protocols for real-life applications is very difficult [2,3]. On the other hand, NP properties critically depend on their composition, shape, size, size distribution, and degree of aggregation [4]. These parameters might be easily affected by the experimental conditions like variation of "room" temperature, presence of dust in the reaction mixture or any impurities in initial chemical reagents [5]. Moreover, the most widely used wet-chemical procedures might require laborious post-synthetic purification of obtained NPs from excess of the reducing and stabilizing reagents [2]. A promising synthetic approach allowing to avoid the purification problem is physical vapor deposition (PVD) of metals onto low vapor pressure liquids [6–8]. Dispersions of NPs obtained by this method are ultra-pure because their composition includes two components: the deposited material forming NPs and the host liquid playing a role of a disperse media and, eventually, a capping agent for the NPs. A liquid was used as a substrate for PVD process, for the first time in 1974 when Yatsuya et al. performed a vacuum evaporation of aluminum onto running silicon oil [9]. The method called VEROS (vacuum evaporation on running oil substrate) was used for production of "extremely fine particles" (less than 10 nm in diameter) made of Al [9] and Ag [10]. In 1996, two different research groups started working onto magnetron sputter deposition of metals onto silicon oils. Ye et al. reported the formation of silver films onto oil surface [11] while Wagener and co-workers managed to produce Ag and Fe NPs in silicon oils under different experimental conditions [12]. Finally, in 2006, Torimoto et al. obtained highly monodisperse Au NPs via direct current magnetron sputtering (DC-MS) of gold onto a thin layer of imidazolium based ionic liquids [13] and initiated series of researches focused onto deposition of various metals on different low vapor pressure liquid

substrates [6,7]. Because "magnetron sputtering onto liquid" procedure is automated in terms of delivery of sputtered species to the solution and takes place inside a closed reactor commonly filled in with inert gas, it got reputation of well-reproducible method of synthesis of high-purity and (relatively) well-dispersed NPs [14,15]. It should be noticed that replicating a synthesis protocol, in this case, might also be difficult task because research groups use different magnetron sputter apparatus, and often the full range of experimental parameters that would allow repeating the published experiment is lacking. Transferring a "deposition recipe" from one process chamber to another is not an easy because the plasma characteristics usually show a non-linear dependence on the various process parameters e.g. magnetic field architecture of the magnetron cathode, sputter target to liquid surface distance and working pressure, etc. As a result, the plasma properties and therefore the NPs obtained at close experimental conditions (gas pressure, discharge voltage/current, etc.) but in different vacuum chambers might have different sizes and size distributions. Moreover, despite the magnetron sputtering-onto-liquids field has been under constant study during last 15 years [6–8], the mechanism of NP formations is still unclear and more quantitative studies focused onto interactions between sputtering plasmas and liquid substrates are required.

In the present article, we discuss the magnetron sputtering of silver onto castor oil. This combination of sputtered material and host liquid has been already used by Wender et al. [16] but as most of the initial works in the sputtering-onto-liquids field, the experiments were done in so-called sputter coaters [13,14,16–21] which do not allow to work under low working pressure and high values of sputter power or voltages. The main goal of the present research is to extend the range of experimental conditions reported by Wender et al. [16] by carrying out deposition inside a full-size vacuum chamber dedicated to magnetron sputter deposition and systematically check the

effect of the sputtering parameters (applied power, working gas pressure, sputter time, type of sputtering plasma) onto properties and stability of Ag NPs.

EXPERIMENTAL PART

The schematic view of the vacuum chamber utilized for the sample preparation is presented on Fig. 1. For the sputtering experiments with liquid substrates, the main deposition chamber (cylinder shape, 25 cm in diameter, 44 cm in height) was permanently pumped with help of the turbomolecular pumps (EBARA ET300W) until a pressure down to 10^{-8} Torr (~10^{-6} Pa) was reached. 5 ml of castor oil (CAS number 8001-79-4; Alfa Aeser) was poured into a cylindrical plastic beaker (2.8 cm in diameter, 3 cm in height), the beaker was placed inside the load-lock chamber, in the holder of a transfer arm. The load lock chamber was then pumped down in two steps. First, the primary pump (PFEIFFER VACUUM DUO line) was turned on to achieve a residual pressure of 10^{-2} Torr (~1.3 Pa). The outgassing process taking place during opening the valve placed in front of the primary pump lasted about 30 minutes. Finally, the turbomolecular pump (LEYBOLD TURBOVAC) allowed to reach pressure of 10^{-7} Torr (~10^{-5} Pa). After this, the separating valve located between the main deposition chamber and the load-lock chamber was opened and the high-purity argon gas was then injected in the chamber. The flow was 30 standard cubic centimeter per minute (sccm) and was controlled via a digital mass flow controller. To reach the setpoint pressure, a throttle valve, set in front of the turbomolecular pump, regulated the pumping speed. Before each deposition run, the surface of the silver target (99.99%; 2-inch (5.08 cm) in diameter; 0.25-inch (0.635 cm) in thickness; Kurt J. Lesker Company Ltd.) was sputter-cleaned in an argon plasma. After stabilization of the target surface chemistry, as verified by monitoring the target current and voltage displayed by the electric DC power supply (Advanced Energy MDX 500), the plasma was turned off and the beaker

containing degassed castor oil was inserted inside the deposition chamber under the center of the silver target. The liquid surface was located at 20 cm from the magnetron cathode surface which was holding the target to be sputtered (Fig. 1). The cathode is furnished with a pair of permanent magnets allowing to trap the plasma near the sputtering target surface. After choosing the experimental conditions, the plasma was turned on for the desired time. During the magnetron sputtering experiments with a bipolar HiPIMS power supply (a prototype constructed in MATERIA NOVA R&D center, Mons, Belgium [22]), at the beginning the plasma with desired parameters of voltage and currents was created inside the main chamber and after the sample was placed into it by the transfer arm and left there for a required time. Depositions with HiPIMS power supply were carried out at argon pressure of 5 mTorr (0.67 Pa), during 45 minutes, at a time-averaged sputter power of 80 W (current 145 mA ; voltage -550 V) with applied positive voltage of 0V (B-HiPIMS_0), +30V (B-HiPIMS_30) and +300 V (B-HiPIMS_300), and the following pulses parameters (800 Hz, 1st negative pulse – 20 µs, 2nd positive pulse – 250 µs, delay between pulses - 10µs). The purpose of applying a positive voltage, hence the name bipolar, is to accelerate the ionized silver atoms.

After the end of each deposition run, the sample was moved back to the load-lock chamber, the separation valve between chambers was closed, the load-lock chamber was vented, and the sample was taken out. Obtained product was photographed and then stirred at the magnetic stirrer for 15 minutes. The resulting solution of Ag NPs was placed inside the 1 cm quartz cell (Hellma 100-QX) and analyzed by UV-vis spectroscopy using Agilent Cary 5000 UV-vis-NIR spectrometer. The cell containing pure castor oil was always used as a reference sample. At the breaks between characterization procedures, all samples were stored in the dark place, in air, at the room temperature.

To be able to compare the results of experiments, carried out at different plasma conditions, the metal flux (the mass of deposited material per unit time and surface) was determined by weighting a thin glass substrate i.e. microscopy glass slide, onto which the material was sputtered for a given duration of time. The results are reported on Fig. 2. The corresponding data are display on Table S1-S2 in the Supporting Information with the obtained flux values for DC-MS and HiPIMS plasmas. As expected, the silver flux linearly increases with the sputter power at fixed argon pressure and exponentially decreases at fixed applied power due to increased gas phase scattering of the sputtered silver atoms as the pressure is increased [23,24].

Images of Ag NP aggregates in castor oil were obtained with a field emission gun scanning electron microscope (FEG-SEM, Hitachi SU8020, Ri Li, Japan). Sample preparation included a dilution of Ag NPs dispersion in castor oil by hot ethanol in a ratio 1/100 with subsequent application of one drop of obtained solution on the 3-mm in diameter copper grid mesh which was put inside the microscope chamber after evaporation of ethanol.

The morphology of the individual Ag NPs was monitored using a JEOL 2200 FS transmission electron microscope (TEM) with an acceleration voltage of 200 kV. The TEM grids were prepared according the procedure described in details in [25].

In order to confirm that castor oil was not degraded due to the plasma exposure, the substate has been studied before and after performing magnetron sputtering by Positive-ion Matrix assisted Laser Desorption/Ionization-Mass Spectrometry (MALDI-MS) experiments which were performed using a Waters QToF Premier mass spectrometer equipped with a Nd:YAG laser operating at 355 nm (third harmonic) with a maximum output of 65 μJ delivered to the sample in 2.2 ns pulses at 50 Hz repeating rate. Time-of-flight mass analysis was performed in the

reflectron mode at a resolution of about 10k (m/z 569). All samples were analyzed using trans-2-[3-(4-tert-butylphenyl)-2-methylprop-2-enylidene]malononitrile (DCTB) as a matrix. Castor oil samples were dissolved in THF to obtain 1 $mg \cdot mL^{-1}$ solution. Additionally, 20 µL of 2 $mg \cdot mL^{-1}$ NaI solution in acetonitrile was added to the oil solution as cationizing agent.

To get further insights into the chemical interactions between the castor oil and the Ag NPs, quantum-chemical calculations were carried out at the density functional theory (DFT) and density functional tight-binding (DFTB) levels in 2 steps. First, a molecular dynamic was applied for the molecule on the frozen silver surface at the DFTB level. We used the 18.2 version of the DFTB+ code [26] with the available hyb+mio Slater-Koster sets [27]. The dynamic time was 20 ps using a Nosé-Hoover thermostat with T = 298 K. The silver metal surface was generated from the bulk using orthogonal unit cells, with enough surface area to prevent intermolecular interactions on the surface. The face centred cubic structure with lattice parameters of a = 4.09 Å was used to model a 3-layer slab exposing the (111) surface with area of 28.9 × 20.0 $Å^2$. For the sake of computational facility, a simplified version of the main castor oil component, 1/3 part of trygliceride of ricinoleic acid (see Fig. S3) was used as a model molecule. The last geometry obtained after the DFTB dynamic was used for DFT based Self-Consistent Field (SCF) energy calculations using the SIESTA 4.1 code [28]. The exchange−correlation functional is described within the general gradient approximation using the Perdew−Burke−Ersenoff (PBE) functional [29]. A double-ζ polarized numerical atomic basis set is adopted for the valence electrons with a mesh cutoff of 250 Ry for the real space grid, whereas core electrons are described with Troullier−Martin pseudopotentials [30]. Considering the size of the system, the energy calculations were done on the Γ point only. The interaction energy, E_{int}, was calculated using the expression: $E_{int} = E_{surf/PE} - [E_{PE} + E_{surf}]$, where $E_{surf/PE}$ is the energy of the full system and E_{PE} and E_{surf} are the

energies of the isolated molecule and the surface in their interface geometries, respectively. To be sure that this DFTB+DFT approach provides trusted results, an additional modelling for a citric acid molecule placed onto the same silver surface was done since citrate anion is a widely used capping agent for Ag NPs [31].

RESULTS AND DISCUSSION

Time evolution of Ag NPs dispersions in castor oil. The combination of silver target and castor oil as a host liquid was chosen as a model system for studying magnetron sputtering onto liquids because of optical characteristics of Ag NPs and oil chemical composition. The strong plasmonic properties of Ag NPs allow to quickly estimate the success of sputter deposition by a naked eye and to characterize the obtained product by UV-vis spectroscopy [32]. Castor oil, that mostly consists of triglyceride of ricinoleic acid [33], should be a good stabilizing agent for the formed metal NPs because of the presence of hydroxyl group on carbon 12 in ricinoleic acid fragment (Fig. 3) [16,18,34]. To the best of our knowledge, castor oil has been used as a stabilizer or/and disperse media for Ag NPs only once in the frame of a sputtering onto liquid [16] and twice during laser ablation processes [35,36]; according to authors, obtained dispersions of Ag NPs were stable during 2-3 month.

In the frame of the present study, the first observations of Ag NPs obtained via magnetron sputtering onto the oil were done by a naked eye. The typical image of the sample taken from vacuum chamber might be found at Fig. 4. The top part of the beaker, which was not hidden inside the sample holder, is covered by a silver film on its inside and outside while the castor oil containing the brown cloud-like area of formed Ag NPs underneath the liquid surface might be seen through the walls of the bottom part of the beaker. The thickness of the silver coating and

the volume occupied by the NP cloud was proportional to the flux of silver atoms and to the sputter time. The thickness of the castor oil layer was 1.5 cm and allowed to see the migration of the NPs inside the host liquid after the magnetron sputtering process (Fig. 4). With time, the deposited concentrated cloud of Ag NPs moved to the bottom of the beaker because of the gravity force. After 3 days of storage on air, NPs partially diffused into the castor oil, but the concentration gradient can still be seen. The slow rate of the diffusion process might be explained by the high viscosity of the castor oil (0.650 Pa·s) [33]. Because the sample left after sputtering for several days in the vacuum chamber, under the pressure 10^{-7} Torr, demonstrated the same behavior and UV-vis spectrum (Fig. S1), it can be concluded that storage in air does not affect the stability of obtained NPs.

After venting the load-lock chamber and picking out the plasma-treated liquid, the samples, previously used for studying the effect of plasma parameters, were stirred. Stability of obtained colloidal dispersions was analyzed by UV-vis spectroscopy. The typical changes in the spectrum of Ag NPs in castor oil during the storage period are shown on Fig. 5a. The presence of a strong surface plasmon resonance (SPR) band with the maximum located between 420 nm - 435 nm (depending on the sputtering conditions) indicates the presence of Ag NPs with diameter larger than 2 nm [37,38]. Obtained UV-vis spectra correspond to the absorbance data provided for Ag NPs produced in castor oil by magnetron sputtering [16] and laser ablation [35,36]. The broad SPR band might be explained by the formation of NPs with broad size distribution or by aggregation of small primary particles [4,39]. With time, the extinction in the region 350-500 nm decreases despite the slow diffusion of NPs in the viscous oil. Such behavior indicates the low colloidal stability of Ag NPs in castor oil media. According to Wender et al. [16], colloidal solutions were stable during three months but, in the present study, we have detected at least 30% decrease of absorbance for

each sample in the 24 hours period following sample preparation. No precipitation or film formation on the walls of the cells has been noticed but probably the absorbance is reduced due to aggregation. The first STEM screening has shown the presence of the NP aggregates with size of several microns (Fig. 5b). It must be noticed that the usage of castor oil as a disperse media requires dilutions of samples with ethanol for electron microscopy characterization which might ultimately induce (further) aggregation of Ag NPs during preparations of microscopy grids for analysis. All TEM images provided in this paper were obtained several months after production of Ag NPs, hence most of the collisions between primary formed NPs had happen [40] and big particles are present on microphotographs.

In order to discard the assumption of stability loss of the colloidal suspension due to a degradation of the castor oil submitted to the magnetron plasma, the substrate has been characterized by MALDI-mass spectrometry before and after plasma treatment. It was shown that the structure and composition of the host liquid hasn't been changed due to interaction with sputter plasmas even during the long sputter times (45 minutes). Indeed, there is no significant modifications of the mass spectra as presented in Fig. S2. Then, the quantum chemistry calculations on DFT and DFTB levels were performed with aim to understand better the chemistry between main castor oil component (triglyceride of ricinoleic acid) and the surface of Ag NPs (see Fig. S3). The positive value of interaction energy (+0.16 eV) means that chemical interactions between NP surface and castor oil triglycerides are not favorable; for example, in case of stable systems, like Ag NPs capped by citric acid, the interaction energy is always negative (-0.19 eV). This explains the low stability of obtained NPs in castor oil solutions.

Effect of sputter time. It can be seen by a naked eye that increasing the sputter time leads to increasing of the concentration of Ag NPs formed under the castor oil surface after magnetron

deposition (Fig. S3). Absorbance of solutions obtained after stirring the plasma treated oil is proportional to the sputter time (Fig. 6a), this relation stays constant during the sample aging. According to publications [6,13,41,42], increasing the sputtering time has no effect on the size and shape of the initial NPs and only changes the concentration of metal in the solution. It is well known that the characteristic SPR bands of Ag NPs are strongly dependent on the size, shape and size distributions of NPs as well as the nature of the surrounding media [4,32,39,43]. The fact that normalized UV-vis spectra (divided by the highest absorbance value) of Ag NP dispersions obtained by DC-MS after 3 min and 5 min sputtering period have the same shape and positions of SPR maxima confirms that varying the sputter time changes only the concentrations of sputter material (Fig. 6 (b, e)).

It was noticed that the shape of the SPR band of all samples obtained at 0.5 mTorr pressure is asymmetrical because of the shoulder at 400 nm. SPR bands with maxima at 402 nm and 435 nm were clearly observed in UV-vis spectra one month after sample synthesis. It means that Ag NPs having a broad size distribution are present in the solutions. TEM images presented in Fig. 6 show the presence of particles with sizes ranging from 1 to 31 nm. The size distribution for samples obtained for 3 min and 5 min sputter times are the same. This result proves, one more time, that sputter time does not affect the size of NPs obtained during magnetron sputtering onto liquids, in our working conditions.

Effect of sputter power. The experiment was planed in order to deposit exactly the same amount of silver i.e. as the sputter power is increased, and consequently the flux of sputtered silver increased, the duration is reduced to reach a constant amount of silver inside the host liquid. Because of the low stability of colloidal dispersions obtained, UV-vis spectra present different absorbance values (Fig. S5a). The maximum of absorbance devided by sputter time is

directly proportional to the sputter power (Fig. S5c). This result is explained by the linear increase of the flux with increasing the sputter power (Fig. 2a). In the normalized UV-vis spectra of Ag NPs dispersions, the SPR bands (Fig. S5 (d, f)) have the same shape and position. This result infers that changing of sputter power changes only the concentration of metal but not the size distributions and shape of produced NPs in the present deposition conditions.

It has been noticed by different research groups that the variations of the discharge current does not affect the formation of gold NPs in ionic liquid BMIM–BF_4 [44], palladium NPs in (HSE)MIM–TFSI [45], or gold NPs in PEG [46]. We agree with Hatakeyama et al [44] that increasing of the NP size with discharge current or voltage noticed by some researchers [16,18,47,48] might be caused by heating the top part of the host liquid by the plasma species and/or the IR radiations emitted by hot, uncooled, sputter target of their sputter coaters used for the deposition metals onto liquids. As reported in [49], energy fluxes in the range of several tens of mW/cm^2 are commonly measured at the substrate surface during magnetron sputter deposition experiments. In our case, we did not notice any significant effect of the sputter power on the size of primary NPs, whose mean diameter was around 2.1-3.1 nm (Fig. 7). This might be explained by the fact that in our case there might be not a dramatic variation of the liquid surface temperature as the deposition time was reduced as the sputter power was increased i.e. the total amount of energy delivered to the liquid was kept roughly constant.

Effect of Argon pressure. The effect of working gas pressure on magnetron sputtering onto liquids was studied only by Wagener at al. [12,50,51] who demonstrated that the size of Ag NPs deposited onto running silicon oil increased from 5 to 20 nm with increasing the pressure from 1 to 30 Pa (0.7 mTorr to 22.5 mTorr, respectively). Authors also mentioned that the number of particles in the suspension strongly decreased due to decreasing of the metal flux with increasing

gas pressure (Fig. 2b). We have noticed the same effect: color intensity and density of the "cloud" containing Ag NPs was much less in case of 15 mTorr pressure as compared to 0.5 mTorr deposition runs, despite the sputter time was 11 times longer (see Fig. S6) in order to keep the amount of deposited silver atoms identical. It might be explained by the fact that, at the lower pressure of 0.5 mTorr, the deposition was done in the "ballistic" regime when atoms take a straight path from target to substrate, i.e. they don't lose their kinetic energy in gas phase collisions. The sputter atoms kinetic energy typically lies in the range of a few eV in the case of magnetron sputter deposition. As the pressure is increased, a larger amount of silver on the outside and the walls of the beaker was noticed after deposition, leading to the conclusion that due to the increased amount of collisions in the gas phase, the atoms ejected from the target take an indirect route to the substrate and there is a lower probability of them landing on the castor oil surface. It should be noticed that all samples obtained at a pressure of 5 or 15 mTorr were more stable than those obtained at a pressure of 0.5 mTorr. After 45 days of storage the decrease of the absorbance at the maximum of SPR band was 85% for 0.5 mTorr, 20% for 5 mTorr and 15% for 15 mTorr. The position of SPR maximum was blue-shifted (426 nm for 5 and 15 mTorr working pressures instead of 435 nm for 0.5 mTorr, see Fig. 8a) and the shape of SPR band were more symmetric i.e. no second peak with maximum at 402 nm was observed for higher pressures within the storage time (Fig. 8c). According to TEM images (Fig. 8 d-g) the mean size of primary NPs slightly increased with argon pressure (from 2.1 nm to 2.8 nm) and the size distribution of all obtained NPs became narrower. This result explains the shape of UV-vis spectra of solutions obtained at higher pressures. It is interesting to compare Ag NPs produced in a frame of this work (15 mTorr pressure, 80 W, 283 V, 280 mA) with particles described by Wender at al.[16] (Bal-tec MED 020 (Irchel) sputter coater, 15 mTorr argon pressure, 280 V and

320 V). In both cases Ag NPs have a spherical shape, the mean size of final NPs was 5.5. nm. Difference in SPR maximum positions, 426 nm (this work) vs. 452 nm (paper[16]) might be explained by different percentage of aggregated Ag NPs produced in different sputter devices.

Effect of the plasma type: DC-MS vs HiPIMS. The main reason for using an HiPIMS power supply was coming from the question: how the kinetic energy and type of sputtered species affect the properties of the metal NPs? In case of sputtering onto liquids, most of the works were done in DC-MS mode, where the sputtered species are neutral atoms with a kinetic energy typically in the range of a few eV or less [23]. In case of HiPIMS plasmas, sputtered species are not only metal atoms but also metal ions [52], and these metal ions have a kinetic energy in the range of few tens of eV. In the frame of bipolar HiPIMS, applying a positive voltage pulse after the negative voltage pulse allows to further accelerate the metal ions. It has been demonstrated that the singly charged metal ions gain a kinetic energy close to the applied positive potential [53]. Such high kinetic energy of the sputtered species might dramatically affect their interaction with the liquid surface, leading to the penetration of ions or/and atoms under the surface of the host liquid and cause the heating up of the liquid surface. To the best of our knowledge only one research group has compared DC-MS and (unipolar) HiPIMS power supplies when Cr-Mn-Fe-Co-Ni alloy was sputtered onto BMIM-TFSI ionic liquid [54]. In case of DC-MS power supply, primary NPs were amorphous, while the usage of the HiPIMS power supply allowed to deposit already crystalline NPs with bigger diameter. Authors suggested that interactions between liquid surface and ionized sputtered species having high kinetic energy affected the nucleation and growth processes and allowed to form crystalline phases at lower temperatures [54]. During the sputtering of silver onto castor oil in HiPIMS regime, the first difference with the DC-MS counterpart was observed by naked eye: there was a visible suspension of brown Ag NP agglomerates in the host

liquid (Fig. S7). Long term stirring of the samples and treatment in an ultrasound bath did not result in the breaking of the aggregates. Thus, all samples obtained with the HiPIMS plasma demonstrate a higher absorption at the region between 550-650 nm due to the presence of aggregated Ag NPs (Fig. 9). Despite the formation of aggregates, these samples have a better stability than Ag NP dispersions obtained with DC-power supply. The position of the SPR resonance maximum was blue-shifted (426 nm for DC-MS; 423 nm for HiPIMS). It should mean that smaller primary Ag NPs are formed in this case. UV-vis spectroscopy has shown that a higher amount of silver was sputtered onto liquid with HiPIMS power supply than thought from the flux calculations (Table S2). It is believed that due to the high kinetic energy of the target atoms in the bipolar HiPIMS regime, atoms incident on the glass used for the weight measurements may have sputtered off some atoms deposited on the glass, hence leading to an underestimation of the deposition flux. In the case of the beaker containing castor oil, (part of) the high-kinetic energy atoms that would sputter off the already deposited atoms are, instead, trapped inside the castor oil solution. In case of HiPIMS, there might also be a dramatic difference in the interactions between the sputtered species and the liquid surface because of the high kinetic energy of silver ions, Ag^+. The positive voltage applied at the cathode, in the HiPIMS mode, allows to accelerate the sputtered metal species towards the substrate to kinetic energy as high as the positive voltage value i.e. +30 or +300 eV (samples B-HiPIMS_30 and B-HiPIMS_300). These accelerated species may penetrate under the liquid surface, dissipate their energy inside the liquid and make the liquid surface heat up. In theory, these high-kinetic energy ions also might damage the molecules of the host liquid, but mass-spectrometry analyses of the samples obtained in DC-MS and HiPIMS regimes have not shown any signs in the changing of castor oil composition (Fig. S2). As it might been seen on TEM images (Fig. 10), the number of

particles with sizes larger than 20 nm are higher in case of usage of the HiPIMS power supply (0.1% for DC-MS, 1.3 % for classical HiPIMS (B-HiPIMS_0) and 4.2% for bipolar HiPIMS (B-HiPIMS_300). It might be explained by the fact that an increase of the temperature of the top layer of castor oil was higher due to the heating by sputtered plasma in HiPIMS mode, a phenomenon that is more pronounced than in case of DC-MS. It is well-known that substrate temperature increases during magnetron sputter deposition [49,55]Since the magnetron sputtering was done on still oil, without stirring and additional cooling of the beaker containing host liquid, the temperature of the liquid surface approximately increased up to 70 °C during 13,5 min deposition in DC-MS mode (13,5 min) and up to 85 °C during 45 min deposition with B-HiPIMS power supply (this approximations were done based on heat flux data from studies [49,56]). It has been already shown that magnetron sputtering onto heated host liquid allows to produce NPs with larger diameter. For example, size of gold NPs increased with temperature of ionic liquid BMIM-BF_4[57] and PEG [40,58], the decrease of the viscosity with the raise in temperature was invoked to explain this observation. Kinetics of NP aggregation depends on the NP diffusion ability [14] which is much higher in case of low viscosity media [59]. Thus, heating of the liquid surface by HiPIMS plasma reduced the viscosity of the top layer of the castor oil (709.1 mm^2/s at 25 °C; 56.1 mm^2/s at °70 C (DC-MS, 15 min) and 31.9 mm^2/s at °85 C (B-HiPIMS, 45 min) according to [60]) and hence the higher number of the collision between primary Ag NPs took place and bigger aggregated particles were formed. This result shows that depositing with HiPIMS power supply might be an alternative to the annealing processes used for increasing the size of primary sputtered NPs [25,54,61,62].

CONCLUSIONS

Silver was sputtered onto liquid substrate, highly available castor oil, using low-pressure magnetron argon-based plasma. The following experimental parameters were varied in order to collect more information about the formation of Ag NPs. It has been clearly shown that, in case of sputtering onto liquid, a cloud with high concentration of Ag NPs forms under the oil surface. The volume occupied by this cloud is proportional to the flux of sputtered atoms and to the deposition time. As it was shown by quantum chemistry-based calculations, the chemical interactions between castor oil triglycerides and silver surfaces are not favorable and would lead to a low colloidal stability of the Ag NPs in castor oil. The size and size distribution of particles do not depend on sputter time and applied sputter power. An increase of sputter pressure from 0.5 mTorr to 15 mTorr leads a slight increase of the size of primary silver NPs from (2.1±0.8) nm to (2.8±1.2) nm and to the set of NPs having narrower size distribution. Applying a bipolar HiPIMS power supply allows to get larger Ag NPs than with DC-MS power supply at the same working pressure and (time-averaged) power and might be used as an alternative to the annealing processes.

ASSOCIATED CONTENT

Supporting Information includes tables with flux values, photographs of the samples obtained at different experimental conditions, UV-vis spectra of Ag NPs solutions in castor oil, DFT/DFTB data and mass-spectroscopy data. The following file (PDF) is available free of charge.

AUTHOR INFORMATION

Corresponding Authors

* Stéphanos Konstantinidis: stephanos.konstantinidis@umons.ac.be;

Anastasiya Sergievskaya: anastasiya.sergievskaya@umons.ac.be

Present Addresses

†If an author's address is different than the one given in the affiliation line, this information may be included here. Amy and Adriano can add something information about new job positions here

Author Contributions

The manuscript was written through contributions of all authors. All authors have given approval to the final version of the manuscript.

Funding Sources

Fonds National de la Recherche Scientifique (F.R.S.-FNRS, Belgium)

Notes

Any additional relevant notes should be placed here.

ACKNOWLEDGMENT

S. Konstantinidis and J. Cornil are senior research associate and research director of the National Fund for Scientific Research (FNRS, Belgium), respectively. S. Konstantinidis and A. Sergievskaya thank the FNRS for the financial support through the "SOLUTIoN" project No T.0134.19. The DFT calculations were supported by the Consortium des Équipements de Calcul Intensif (CÉCI), funded by the Fonds National de la Recherche Scientifique (F. R. S.-FNRS) under Grant No. 2.5020.11. The S²MOs lab is grateful to the Fonds National de la Recherche Scientifique (F. R. S.-FNRS) for financial support for the acquisition of the Waters QTof Premier mass spectrometer. A. Chauvin acknowledges financial support from the project

"Nanomaterials centre for advanced applications", Project No. CZ.02.1.01/0.0/0.0/15_003/0000485, financed by ERDF. A. Sergievskaya would like to thank Dany Cornelissen for his invaluable help with vacuum chamber construction and practical advices.

ABBREVIATIONS

DC-MS, direct current magnetron sputtering; HiPIMS, high-power impulse magnetron sputtering; NP, nanoparticle; TEM, transmission electron microscopy; DFT, density functional theory; DFTB, density functional tight-binding; MALDI-MS, Positive-ion Matrix assisted Laser Desorption/Ionization-Mass Spectrometry.

REFERENCES

(1) *Nanoparticles: From Theory to Application*, 2nd, Compl ed.; Schmid, G., Ed.; Weinheim: Wiley-VCH Verlag GmbH & Co. KGaA, 2010.

(2) Sebastian, V.; Arruebo, M.; Santamaria, J. Reaction Engineering Strategies for the Production of Inorganic Nanomaterials. *Small* **2014**, *10* (5), 835–853. https://doi.org/10.1002/smll.201301641.

(3) Panariello, L.; Damilos, S.; Du Toit, H.; Wu, G.; Radhakrishnan, A. N. P.; Parkin, I. P.; Gavriilidis, A. Highly Reproducible, High-Yield Flow Synthesis of Gold Nanoparticles Based on a Rational Reactor Design Exploiting the Reduction of Passivated Au(Iii). *React. Chem. Eng.* **2020**, *5* (4), 663–676. https://doi.org/10.1039/c9re00469f.

(4) Liz-Marzán, L. M. Nanometals: Formation and Color. *Mater. Today* **2004**, *7* (2), 26–31. https://doi.org/10.1016/S1369-7021(04)00080-X.

(5) Liz-Marzán, L. M.; Kagan, C. R.; Millstone, J. E. Reproducibility in Nanocrystal Synthesis? Watch Out for Impurities! *ACS Nano* **2020**, *14* (6), 6359–6361. https://doi.org/10.1021/acsnano.0c04709.

(6) Wender, H.; Migowski, P.; Feil, A. F.; Teixeira, S. R.; Dupont, J. Sputtering Deposition of Nanoparticles onto Liquid Substrates: Recent Advances and Future Trends. *Coord. Chem. Rev.* **2013**, *257* (17–18), 2468–2483. https://doi.org/10.1016/j.ccr.2013.01.013.

(7) Nguyen, M. T.; Yonezawa, T. Sputtering onto a Liquid: Interesting Physical Preparation Method for Multi-Metallic Nanoparticles. *Sci. Technol. Adv. Mater.* **2018**, *19* (1), 883–898. https://doi.org/10.1080/14686996.2018.1542926.

(8) Torimoto, T.; Kameyama, T.; Kuwabata, S. Top-Down Synthesis Methods for Nanoscale Catalysts. In *Nanocatalysis in Ionic Liquids*; Wiley-VCH Verlag GmbH & Co. KGaA: Weinheim, Germany, 2016; pp 171–205. https://doi.org/10.1002/9783527693283.ch9.

(9) Yatsuya, S.; Mihama, K.; Uyeda, R. A New Technique for the Preparation of Extremely Fine Metal Particles. *Jpn. J. Appl. Phys.* **1974**, *13* (4), 749–750. https://doi.org/10.1143/JJAP.13.749.

(10) Yatsuya, S.; Tsukasaki, Y.; Mihama, K.; Uyeda, R. Preparation of Extremely Fine Particles by Vacuum Evaporation onto a Running Oil Substrate. *J. Cryst. Growth* **1978**, *45* (C), 490–494. https://doi.org/10.1016/0022-0248(78)90481-5.

(11) Ye, G. X.; Zhang, Q. R.; Feng, C.; Ge, H.; Jiao, Z. Structural and Electrical Properties of a Metallic Rough-Thin-Film System Deposited on Liquid Substrates. *Phys. Rev. B* **1996**, *54* (20), 14754–14757. https://doi.org/10.1103/PhysRevB.54.14754.

(12) Wagener, M.; Murty, B. S.; Günther, B. Preparation of Metal Nanosuspensions by High-Pressure DC-Sputtering on Running Liquids. *MRS Proc.* **1996**, *457*, 149. https://doi.org/10.1557/PROC-457-149.

(13) Torimoto, T.; Okazaki, K. I.; Kiyama, T.; Hirahara, K.; Tanaka, N.; Kuwabata, S. Sputter Deposition onto Ionic Liquids: Simple and Clean Synthesis of Highly Dispersed Ultrafine Metal Nanoparticles. *Appl. Phys. Lett.* **2006**, *89* (24), 243117. https://doi.org/10.1063/1.2404975.

(14) Vanecht, E.; Binnemans, K.; Seo, J. W.; Stappers, L.; Fransaer, J. Growth of Sputter-Deposited Gold Nanoparticles in Ionic Liquids. *Phys. Chem. Chem. Phys.* **2011**, *13* (30),

13565–13571. https://doi.org/10.1039/c1cp20552h.

(15) Carette, X.; Debièvre, B.; Cornil, D.; Cornil, J.; Leclère, P.; Maes, B.; Gautier, N.; Gautron, E.; El Mel, A. A.; Raquez, J. M.; et al. On the Sputtering of Titanium and Silver onto Liquids, Discussing the Formation of Nanoparticles. *J. Phys. Chem. C* **2018**, *122* (46), 26605–26612. https://doi.org/10.1021/acs.jpcc.8b06987.

(16) Wender, H.; Gonçalves, R. V.; Feil, A. F.; Migowski, P.; Poletto, F. S.; Pohlmann, A. R.; Dupont, J.; Teixeira, S. R. Sputtering onto Liquids: From Thin Films to Nanoparticles. *J. Phys. Chem. C* **2011**, *115* (33), 16362–16367. https://doi.org/10.1021/jp205390d.

(17) Tsuda, T.; KURIHARA, T.; HOSHINO, Y.; KIYAMA, T.; OKAZAKI, K.; TORIMOTO, T.; KUWABATA, S. Electrocatalytic Activity of Platinum Nanoparticles Synthesized by Room-Temperature Ionic Liquid-Sputtering Method. *Electrochemistry* **2009**, *77* (8), 693–695. https://doi.org/10.5796/electrochemistry.77.693.

(18) Wender, H.; De Oliveira, L. F.; Feil, A. F.; Lissner, E.; Migowski, P.; Meneghetti, M. R.; Teixeira, S. R.; Dupont, J. Synthesis of Gold Nanoparticles in a Biocompatible Fluid from Sputtering Deposition onto Castor Oil. *Chem. Commun.* **2010**, *46* (37), 7019–7021. https://doi.org/10.1039/c0cc01353f.

(19) Wender, H.; De Oliveira, L. F.; Migowski, P.; Feil, A. F.; Lissner, E.; Prechtl, M. H. G.; Teixeira, S. R.; Dupont, J. Ionic Liquid Surface Composition Controls the Size of Gold Nanoparticles Prepared by Sputtering Deposition. *J. Phys. Chem. C* **2010**, *114* (27), 11764–11768. https://doi.org/10.1021/jp102231x.

(20) Khatri, O. P.; Adachi, K.; Murase, K.; Okazaki, K. I.; Torimoto, T.; Tanaka, N.; Kuwabata, S.; Sugimura, H. Self-Assembly of Ionic Liquid (BMI-PF6)-Stabilized Gold Nanoparticles on a Silicon Surface: Chemical and Structural Aspects. *Langmuir* **2008**, *24* (15), 7785–7792. https://doi.org/10.1021/la800678m.

(21) Shishino, Y.; Yonezawa, T.; Kawai, K.; Nishihara, H. Molten Matrix Sputtering Synthesis of Water-Soluble Luminescent Au Nanoparticles with a Large Stokes Shift. *Chem. Commun.* **2010**, *46* (38), 7211. https://doi.org/10.1039/c0cc01702g.

(22) Britun, N.; Michiels, M.; Godfroid, T.; Snyders, R. Ion Density Evolution in a High-Power Sputtering Discharge with Bipolar Pulsing. *Appl. Phys. Lett.* **2018**, *112* (23), 234103. https://doi.org/10.1063/1.5030697.

(23) Depla, D. *Magnetrons, Reactive Gases and Sputtering*, Third.; 2015.

(24) Wasa, K.; Adachi, H.; Kitabatake, M. *Thin Film Materials Technology: Sputtering of Compound Materials*; 2004.

(25) Chauvin, A.; Sergievskaya, A.; El Mel, A.-A.; Fucikova, A.; Antunes Corrêa, C.; Vesely, J.; Duverger-Nédellec, E.; Cornil, D.; Cornil, J.; Tessier, P.-Y.; et al. Co-Sputtering of Gold and Copper onto Liquids: A Route towards the Production of Porous Gold Nanoparticles. *Nanotechnology* **2020**, *31* (45), 455303. https://doi.org/10.1088/1361-6528/abaa75.

(26) Hourahine, B.; Aradi, B.; Blum, V.; Bonafé, F.; Buccheri, A.; Camacho, C.; Cevallos, C.; Deshaye, M. Y.; Dumitrică, T.; Dominguez, A.; et al. DFTB+, a Software Package for Efficient Approximate Density Functional Theory Based Atomistic Simulations. *J. Chem. Phys.* **2020**, *152* (12), 124101. https://doi.org/10.1063/1.5143190.

(27) Elstner, M.; Porezag, D.; Jungnickel, G.; Elsner, J.; Haugk, M.; Frauenheim, T.; Suhai, S.; Seifert, G. Self-Consistent-Charge Density-Functional Tight-Binding Method for Simulations of Complex Materials Properties. *Phys. Rev. B* **1998**, *58* (11), 7260–7268. https://doi.org/10.1103/PhysRevB.58.7260.

(28) Artacho, E.; Anglada, E.; Diéguez, O.; Gale, J. D.; García, A.; Junquera, J.; Martin, R. M.; Ordejón, P.; Pruneda, J. M.; Sánchez-Portal, D.; et al. The SIESTA Method; Developments and Applicability. *J. Phys. Condens. Matter* **2008**, *20* (6), 064208. https://doi.org/10.1088/0953-8984/20/6/064208.

(29) Perdew, J. P.; Burke, K.; Wang, Y. Generalized Gradient Approximation for the Exchange-Correlation Hole of a Many-Electron System. *Phys. Rev. B* **1996**, *54* (23), 16533–16539. https://doi.org/10.1103/PhysRevB.54.16533.

(30) Troullier, N.; Martins, J. L. Efficient Pseudopotentials for Plane-Wave Calculations. II.

Operators for Fast Iterative Diagonalization. *Phys. Rev. B* **1991**, *43* (11), 8861–8869. https://doi.org/10.1103/PhysRevB.43.8861.

(31) Kilin, D. S.; Prezhdo, O. V.; Xia, Y. Shape-Controlled Synthesis of Silver Nanoparticles: Ab Initio Study of Preferential Surface Coordination with Citric Acid. *Chem. Phys. Lett.* **2008**, *458* (1–3), 113–116. https://doi.org/10.1016/j.cplett.2008.04.046.

(32) Pastoriza-Santos, I.; Liz-Marzán, L. M. Colloidal Silver Nanoplates. State of the Art and Future Challenges. *J. Mater. Chem.* **2008**, *18* (15), 1724. https://doi.org/10.1039/b716538b.

(33) Patel, V. R.; Dumancas, G. G.; Viswanath, L. C. K.; Maples, R.; Subong, B. J. J. Castor Oil: Properties, Uses, and Optimization of Processing Parameters in Commercial Production. *Lipid Insights* **2016**, *9*, LPI.S40233. https://doi.org/10.4137/LPI.S40233.

(34) Fujita, A.; Matsumoto, Y.; Takeuchi, M.; Ryuto, H.; Takaoka, G. H. Growth Behavior of Gold Nanoparticles Synthesized in Unsaturated Fatty Acids by Vacuum Evaporation Methods. *Phys. Chem. Chem. Phys.* **2016**, *18* (7), 5464–5470. https://doi.org/10.1039/C5CP07323E.

(35) Aleali, H.; Mansour, N. Thermal-Induced Nonlinearity Enhancement in Ag Nanoparticles Colloids by Low Thermal Conductivity Liquids. *J. Opt.* **2019**. https://doi.org/10.1007/s12596-019-00520-6.

(36) Zamiri, R.; Zakaria, A.; Abbastabar, H.; Darroudi, M.; Husin, M. S.; Mahdi, M. A. Laser-Fabricated Castor Oil-Capped Silver Nanoparticles. *Int. J. Nanomedicine* **2011**, *6* (1), 565–568. https://doi.org/10.2147/IJN.S16384.

(37) Corpuz, R. D.; Ishida, Y.; Yonezawa, T. Synthesis of Cationically Charged Photoluminescent Coinage Metal Nanoclusters by Sputtering over a Liquid Polymer Matrix. *New J. Chem.* **2017**, *41* (14), 6828–6833. https://doi.org/10.1039/c7nj01369h.

(38) Ishida, Y.; Nakabayashi, R.; Matsubara, M.; Yonezawa, T. Silver Sputtering into a Liquid Matrix Containing Mercaptans: The Systematic Size Control of Silver Nanoparticles in Single Nanometer-Orders. *New J. Chem.* **2015**, *39* (6), 4227–4230.

https://doi.org/10.1039/c5nj00294j.

(39) Panigrahi, S.; Praharaj, S.; Basu, S.; Ghosh, S. K.; Jana, S.; Pande, S.; Vo-dinh, T.; Jiang, H.; Pal, T. Self-Assembly of Silver Nanoparticles : Synthesis , Stabilization , Optical Properties , and Application in Surface-Enhanced Raman Scattering. **2006**, 13436–13444. https://doi.org/https://doi.org/10.1021/jp062119l.

(40) Deng, L.; Nguyen, M. T.; Mei, S.; Tokunaga, T.; Kudo, M.; Matsumura, S.; Yonezawa, T. Preparation and Growth Mechanism of Pt/Cu Alloy Nanoparticles by Sputter Deposition onto a Liquid Polymer. *Langmuir* **2019**, *35*, 8418–8427. https://doi.org/10.1021/acs.langmuir.9b01112.

(41) Tsuda, T.; Yoshii, K.; Torimoto, T.; Kuwabata, S. Oxygen Reduction Catalytic Ability of Platinum Nanoparticles Prepared by Room-Temperature Ionic Liquid-Sputtering Method. *J. Power Sources* **2010**, *195* (18), 5980–5985. https://doi.org/10.1016/j.jpowsour.2009.11.027.

(42) Raghuwanshi, V. S.; Ochmann, M.; Hoell, A.; Polzer, F.; Rademann, K. Deep Eutectic Solvents for the Self-Assembly of Gold Nanoparticles: A SAXS, UV–Vis, and TEM Investigation. *Langmuir* **2014**, *30* (21), 6038–6046. https://doi.org/10.1021/la500979p.

(43) Mulvaney, P. Surface Plasmon Spectroscopy of Nanosized Metal Particles. *Langmuir* **2002**. https://doi.org/10.1021/la9502711.

(44) Hatakeyama, Y.; Onishi, K.; Nishikawa, K. Effects of Sputtering Conditions on Formation of Gold Nanoparticles in Sputter Deposition Technique. *RSC Adv.* **2011**, *1* (9), 1815–1821. https://doi.org/10.1039/c1ra00688f.

(45) Qadir, M. I.; Kauling, A.; Ebeling, G.; Fartmann, M.; Grehl, T.; Dupont, J. Functionalized Ionic Liquids Sputter Decorated with Pd Nanoparticles. *Aust. J. Chem.* **2019**, *72* (2), 49. https://doi.org/10.1071/CH18183.

(46) Sumi, T.; Motono, S.; Ishida, Y.; Shirahata, N.; Yonezawa, T. Formation and Optical Properties of Fluorescent Gold Nanoparticles Obtained by Matrix Sputtering Method with Volatile Mercaptan Molecules in the Vacuum Chamber and Consideration of Their

Structures. *Langmuir* **2015**, *31* (14), 4323–4329. https://doi.org/10.1021/acs.langmuir.5b00294.

(47) SUZUKI, T.; OKAZAKI, K.; KIYAMA, T.; KUWABATA, S.; TORIMOTO, T. A Facile Synthesis of AuAg Alloy Nanoparticles Using a Chemical Reaction Induced by Sputter Deposition of Metal onto Ionic Liquids. *Electrochemistry* **2009**, *77* (8), 636–638. https://doi.org/10.5796/electrochemistry.77.636.

(48) Sugioka, D.; Kameyama, T.; Kuwabata, S.; Torimoto, T. Single-Step Preparation of Two-Dimensionally Organized Gold Particles via Ionic Liquid/Metal Sputter Deposition. *Phys. Chem. Chem. Phys.* **2015**, *17* (19), 13150–13159. https://doi.org/10.1039/c5cp01602a.

(49) Thomann, A.-L. L.; Caillard, A.; Raza, M.; El Mokh, M.; Cormier, P. A. A.; Konstantinidis, S. Energy Flux Measurements during Magnetron Sputter Deposition Processes. *Surf. Coatings Technol.* **2019**, *377* (March), 124887. https://doi.org/10.1016/j.surfcoat.2019.08.016.

(50) Wagener, M.; Günther, B. High Pressure DC-Magnetron Sputtering on Liquids: A New Process for the Production of Metal Nanosuspensions. In *Structure, Dynamics and Properties of Disperse Colloidal Systems*; Steinkopff: Darmstadt, 1998; Vol. 111, pp 78–81.

(51) Wagener, M.; Günther, B. Sputtering on Liquids - A Versatile Process for the Production of Magnetic Suspensions? *J. Magn. Magn. Mater.* **1999**, *201* (1–3), 41–44. https://doi.org/10.1016/S0304-8853(99)00055-4.

(52) Sarakinos, K.; Alami, J.; Konstantinidis, S. High Power Pulsed Magnetron Sputtering: A Review on Scientific and Engineering State of the Art. *Surf. Coatings Technol.* **2010**, *204* (11), 1661–1684. https://doi.org/10.1016/j.surfcoat.2009.11.013.

(53) Keraudy, J.; Viloan, R. P. B.; Raadu, M. A.; Brenning, N.; Lundin, D.; Helmersson, U. Bipolar HiPIMS for Tailoring Ion Energies in Thin Film Deposition. *Surf. Coatings Technol.* **2019**, *359*, 433–437. https://doi.org/10.1016/j.surfcoat.2018.12.090.

(54) Garzón-Manjón, A.; Meyer, H.; Grochla, D.; Löffler, T.; Schuhmann, W.; Ludwig, A.;

Scheu, C. Controlling the Amorphous and Crystalline State of Multinary Alloy Nanoparticles in An Ionic Liquid. *Nanomaterials* **2018**, *8* (11), 903. https://doi.org/10.3390/nano8110903.

(55) Thornton, J. A. Substrate Heating in Cylindrical Magnetron Sputtering Sources. *Thin Solid Films* **1978**, *54* (1), 23–31. https://doi.org/10.1016/0040-6090(78)90273-0.

(56) Cormier, P.-A.; Thomann, A.-L.; Dolique, V.; Balhamri, A.; Dussart, R.; Semmar, N.; Lecas, T.; Brault, P.; Snyders, R.; Konstantinidis, S. IR Emission from the Target during Plasma Magnetron Sputter Deposition. *Thin Solid Films* **2013**, *545*, 44–49. https://doi.org/10.1016/j.tsf.2013.07.025.

(57) Hatakeyama, Y.; Takahashi, S.; Nishikawa, K. Can Temperature Control the Size of Au Nanoparticles Prepared in Ionic Liquids by the Sputter Deposition Technique? *J. Phys. Chem. C* **2010**, *114* (25), 11098–11102. https://doi.org/10.1021/jp102763n.

(58) Hatakeyama, Y.; Morita, T.; Takahashi, S.; Onishi, K.; Nishikawa, K. Synthesis of Gold Nanoparticles in Liquid Polyethylene Glycol by Sputter Deposition and Temperature Effects on Their Size and Shape. *J. Phys. Chem. C* **2011**, *115* (8), 3279–3285. https://doi.org/10.1021/jp110455k.

(59) Mun, E. A.; Hannell, C.; Rogers, S. E.; Hole, P.; Williams, A. C.; Khutoryanskiy, V. V. On the Role of Specific Interactions in the Diffusion of Nanoparticles in Aqueous Polymer Solutions. *Langmuir* **2014**, *30* (1), 308–317. https://doi.org/10.1021/la4029035.

(60) Active Standard ASTM D341 - 20e1- Standard Practice for Viscosity-Temperature Equations and Charts for Liquid Petroleum or Hydrocarbon Products https://www.astm.org/Standards/D341.htm.

(61) Schmitz, A.; Meyer, H.; Meischein, M.; Garzón Manjón, A.; Schmolke, L.; Giesen, B.; Schlüsener, C.; Simon, P.; Grin, Y.; Fischer, R. A.; et al. Synthesis of Plasmonic Fe/Al Nanoparticles in Ionic Liquids. *RSC Adv.* **2020**, *10* (22), 12891–12899. https://doi.org/10.1039/D0RA01111H.

(62) Torimoto, T.; Kameyama, T.; Kuwabata, S. Top-Down Synthesis Methods for Nanoscale

Catalysts. *Nanocatalysis Ion. Liq.* **2016**, 171–205. https://doi.org/10.1002/9783527693283.ch9.

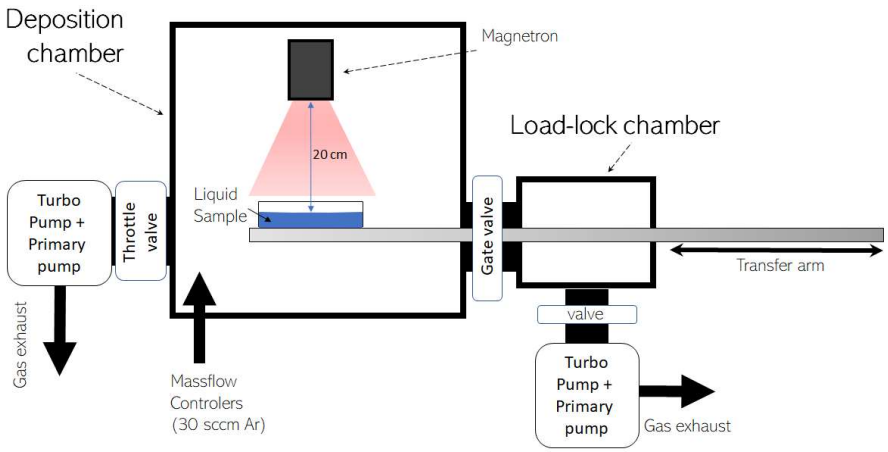

Figure 1. Schematic representation of the vacuum system utilized for the magnetron sputtering of silver onto castor oil.

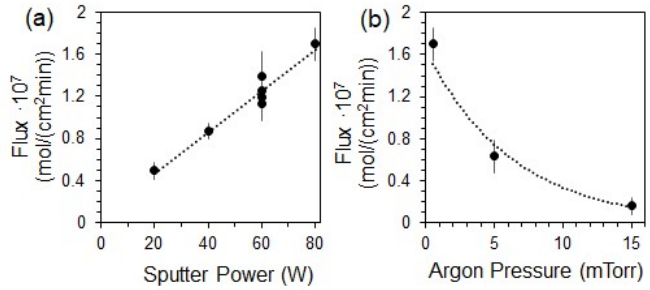

Figure 2. a) Dependence of the silver flux from applied power at fixed argon pressure 0.5 mTorr (0.07 Pa). b) Dependence of the silver flux from working argon pressure at fixed applied power 80 W. All measurements were done with DC power supply.

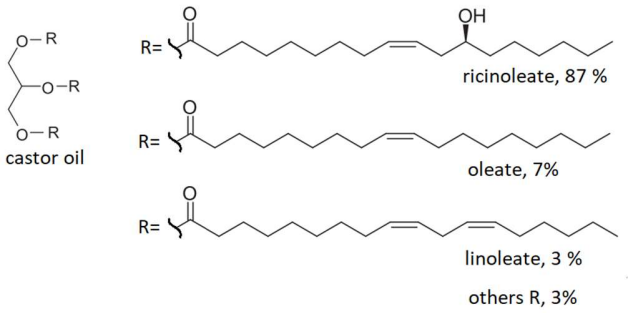

Figure 3. Structures of general triglycerides present in castor oil.

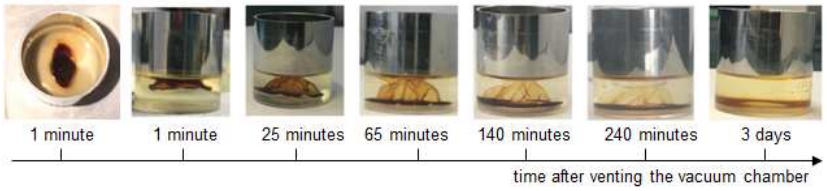

Figure 4. Photographs of the sample of Ag NPs in castor oil (pressure 0.5 mTorr, power 60 W (180 mA; 324 V), time 7 min) at different time after venting the vacuum chamber.

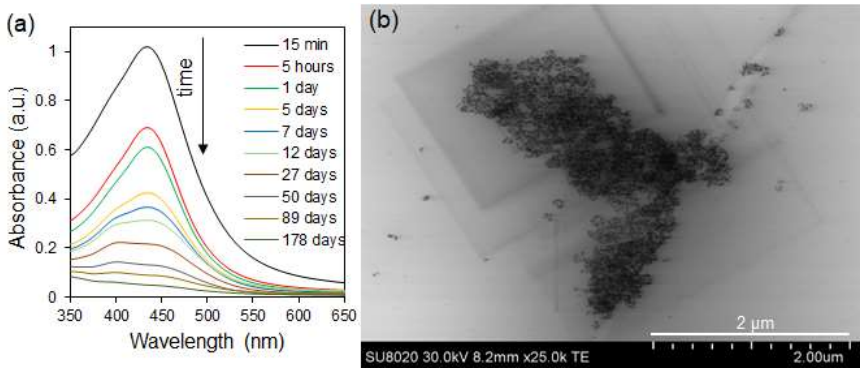

Figure 5. Spectral changes of the solution (a) and STEM image (b) of Ag NPs in castor oil (experimental conditions: pressure 0.5 mTorr, power 80 W (233 mA; 340 V), sputter time 3 min).

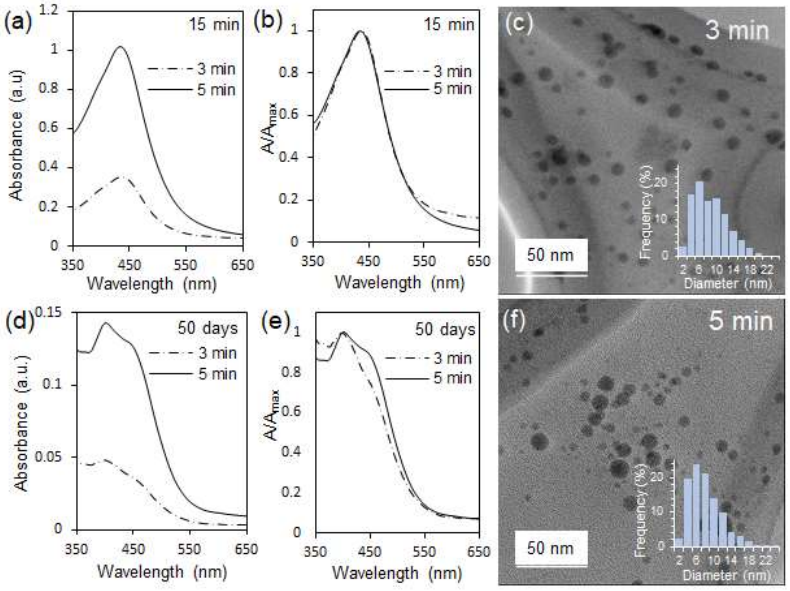

Figure 6. UV-vis spectra of colloidal solutions of Ag NPs in castor oil produced with different sputter times (experimental conditions: pressure 0.5 mTorr, sputter power 80 W (340 V, 233 mA)). Spectra were recorded 15 min after venting the vacuum chamber (a) and 50 days later (d); normalized spectra of the same solutions (b) and (e). TEM images and size distributions of Ag NPs obtained at sputter time 3 min (c) and 5 min (f).

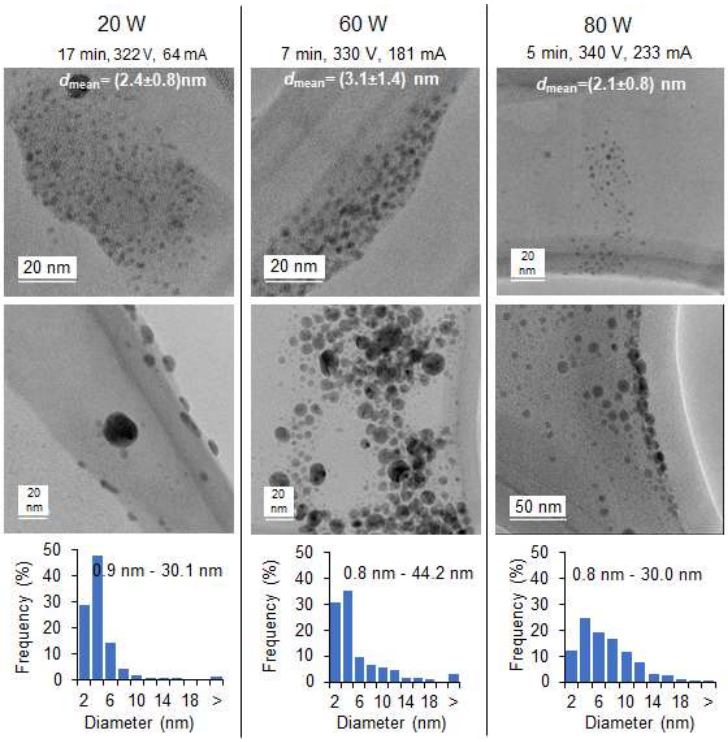

Figure 7. TEM images and size distributions of Ag NPs obtained via DC-MS of silver onto castor oil at fixed argon pressure 0.5 mTorr but different sputter power.

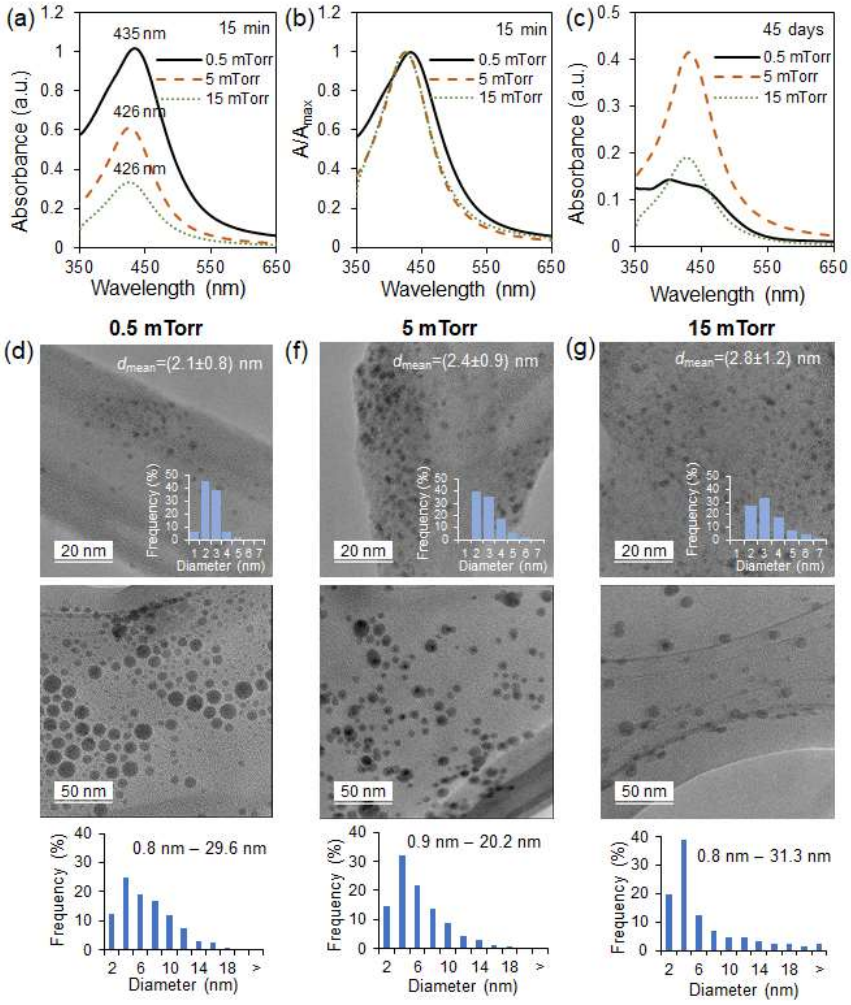

Figure 8. UV-vis spectra of the colloidal solutions of Ag NPs in castor oil obtained at fixed sputter power (80 W) but different argon pressure: (a) spectra 15 min after venting the vacuum chamber, (b) normalized spectra, (c) spectra 45 days after the synthesis. TEM images and size distributions of Ag NPs produced at pressure (d) 0.5 mTorr, (f) 5 mTorr and (g) 15 mTorr.

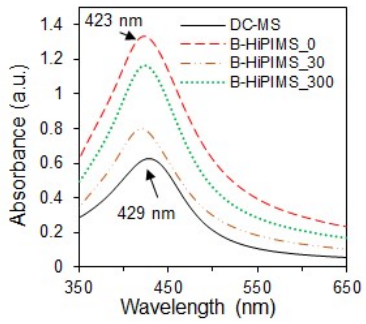

Figure 9. UV-vis spectra of the colloidal solutions of Ag NPs in castor oil obtained with DC-MS and bipolar HiPIMS power supplies, spectra were recorded 15 minutes after venting the vacuum chamber.

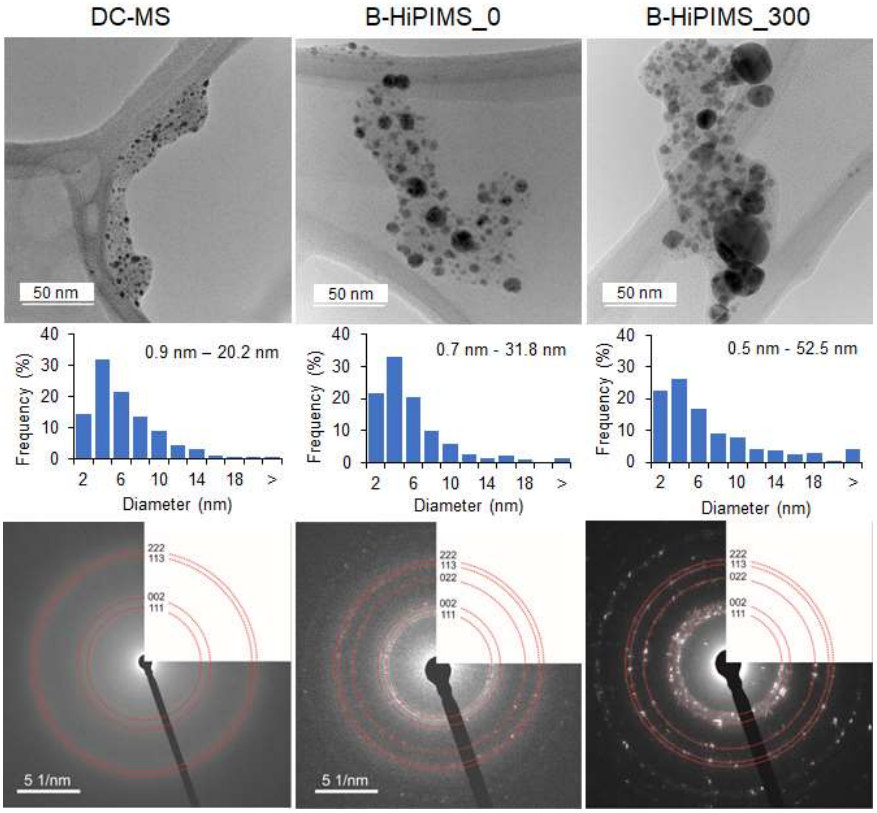

Figure 10. TEM images, size distributions and diffraction patterns of Ag NPs produced with DC-MS (left), HiPIMS (middle) and bipolar HiPIMS (right) power supplies at pressure 5 mTorr and sputter power 80 W.